Hindawi Publishing Corporation
ISRN Astronomy and Astrophysics
Volume 2013, Article ID 281849, 15 pages
http://dx.doi.org/10.1155/2013/281849

Research Article

The Restricted 2+2 Body Problem: Parametric Variation of the Equilibrium States of the Minor Bodies and Their Attracting Regions

Maria N. Croustalloudi and Tilemahos J. Kalvouridis

Department of Mechanics, Faculty of Applied Mathematical and Physical Sciences, National Technical University of Athens, 15773 Athens, Greece

Correspondence should be addressed to Tilemahos J. Kalvouridis; tkalvouridis@gmail.com

Received 29 November 2012; Accepted 17 December 2012

Academic Editors: P. P. Avelino, D. M. Christodoulou, M. Ding, P. A. Hughes, P. Marziani, and R. A. West

The restricted 2+2 body problem was stated by Whipple (1984) as a particular case of the general $n + \nu$ problem described by Whipple and Szebehely (1984). In this work we reconsider the problem by studying some aspects of the dynamics of the minor bodies, such as the parametric variation of their equilibrium positions, as well as the attracting regions formed by the initial approximations used for the numerical determination of these positions. In the latter case we describe the process to form these regions, and we numerically investigate their dependence on the parameters of the system. The results in many cases show a fractal-type structure of these regions. As test problems, we use the Sun-Jupiter-binary asteroids and the Earth-Moon-dual artificial satellites systems.

1. Introduction

After many years of thorough study of the restricted three-body problem and the new issues imposed by the flight missions in the 60s, 70s, and 80s, many investigators have focused their scientific interest to new N-body models ($N > 3$) in order to approximate real celestial systems. The restricted 2+2 body problem, which can be considered as a version of the restricted three-body problem and as a particular case of the $n + \nu$ bodies problem (n major bodies and ν minor ones) where $n = 2$ and $\nu = 2$, belongs to this category.

The original configuration consists of two big spherical, homogeneous bodies P_1 and P_2, called hereafter the primaries, with masses M_1 and M_2, respectively, which rotate around their common center of mass in circular orbits with a constant angular velocity under their mutual gravitational attraction (Figure 1). In the resultant gravitational field created by the primaries, two point-like small bodies, namely, S_1 and S_2, move while mutually attracting each other without perturbing the primaries. According to the formulation given by Whipple [1], the problem is characterized by three parameters μ, μ_1, and μ_2 which are the reduced masses of primary P_2 and of the two minor bodies, respectively.

Among the works treating this problem, we can mention the papers of Whipple and White [2] and Milani and Nobili [3] who applied this model to study the dynamics of binary asteroids in the solar system, as well as the paper of Thanos [4] who studied the case of possible collisions between the minor bodies and proposed a regularization formula for the transformation of the equations of motion similar to the one used in the restricted three-body problem. In the 90s some improved versions of the problem have appeared in the international bibliography. El-Shaboury [5] considered that the 2+2 bodies are homogenous, axisymmetric ellipsoids so that their equatorial planes coincide with the orbital plane of the centers of mass. Michalakis and Mavraganis [6] replaced the two minor point-like masses with two triaxial rigid bodies, Kalvouridis and Mavraganis [7] studied the case where the two primaries are radiating sources, and Mavraganis and Kalvouridis [8] considered the two minor bodies as gyrostats. A little later Kalvouridis [9] assumed that the two primaries are oblate spheroids. Finally, in a completely different version,

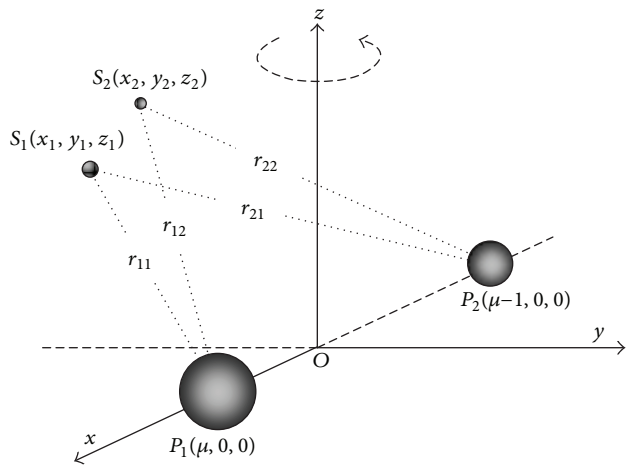

Figure 1: The configuration of the 2+2 body problem.

Prasad and Ishwar [10] studied the same configuration by considering that the primaries are magnetic dipoles and the minor bodies are electric dipoles.

In what follows, we shall numerically investigate some new aspects of the 2+2 body problem including the parametric variation of the equilibrium states (Section 3), as well as the formation, the structure, and the parametric dependence of the attracting regions of these equilibrium states (Section 4). We shall use two test problems; the Sun-Jupiter-binary asteroids system (case A) and an imaginary flying formation mission of a dual satellite system in the Earth-Moon's gravitational field (case B). Our choice is based upon the fact that the physical measures of these two systems present significant differences. All along the study of the attracting regions, and for comparison reasons, we shall also use the restricted three-body problem (RTBP). The data which are used in this work and concern the aforementioned cases are shown in an appendix at the end of the text.

2. Equations of Motion

As we have mentioned before, the system consists of two primaries P_i, $i = 1, 2$, with masses M_1, M_2 ($M_1 \geq M_2$), which revolve in circular orbits around the center of mass, and of two minor bodies S_i, $i = 1, 2$, with masses m_i, $i = 1, 2$, such as $m_i \ll M_j$, $i, j = 1, 2$ (Figure 1). The minor bodies move under the combined action of the primaries and their mutual attraction. The aim of the problem is to describe the dynamical behavior of this pair of minor bodies.

By considering a synodic coordinate system Oxyz, the xy-plane of which coincides with the orbital plane of the primaries, and by taking the axis of syzygy of the primaries as the x-axis, the dimensionless equations of motion of the minor bodies S_1 and S_2 in this system (without loss of generality we may assume that the dimensionless angular velocity of the synodic system is equal to unity) are

$$\begin{aligned} \ddot{x}_i - 2\dot{y}_i &= \frac{1}{\mu_i}\frac{\partial U}{\partial x_i}, \\ \ddot{y}_i + 2\dot{x}_i &= \frac{1}{\mu_i}\frac{\partial U}{\partial y_i}, \\ \ddot{z}_i &= \frac{1}{\mu_i}\frac{\partial U}{\partial z_i}, \end{aligned} \tag{1}$$

(Whipple and Szebehely [11]), where

$$U = \sum_{i=1}^{2}\mu_i\left[\frac{1}{2}\left({x_i}^2 + {y_i}^2\right) + \frac{1-\mu}{r_{1i}} + \frac{\mu}{r_{2i}} + \frac{1}{2}\frac{\mu_{3-i}}{r}\right]. \tag{2}$$

μ is the reduced mass of the smaller primary P_2

$$\begin{aligned} \mu &= \frac{M_2}{M_1 + M_2}, \quad 0 < \mu \leq \frac{1}{2}, \\ \mu_i &= \frac{m_i}{M_1 + M_2}, \quad i = 1, 2. \end{aligned} \tag{3}$$

μ_i are the reduced masses of the minor bodies S_i. Also, r is the distance between the minor bodies and r_{1i}, r_{2i} are their distances from the two primaries, where

$$\begin{aligned} r^2 &= (x_1 - x_2)^2 + (y_1 - y_2)^2 + (z_1 - z_2)^2, \\ r_{1i}^2 &= (x_i - \mu)^2 + {y_i}^2 + {z_i}^2, \\ r_{2i}^2 &= (x_i - \mu + 1)^2 + {y_i}^2 + {z_i}^2, \end{aligned} \tag{4}$$

Here we note that for the normalization process we have used the total mass of the primaries $M_1 + M_2$ and their distance P_1P_2.

There is a Jacobian-type integral of motion

$$2U - \sum_{i=1}^{2}\mu_i\left({\dot{x}_i}^2 + {\dot{y}_i}^2 + {\dot{z}_i}^2\right) = C, \tag{5}$$

which resembles the one of the restricted three-body problem (Szebehely [12]).

3. Equilibrium Positions, Parametric Variation, and Stability

3.1. Distribution of the Equilibrium Positions. Whipple has proved that all equilibrium positions (S_{1e}, S_{2e}) are located on the xy-plane of the synodic system. He also found that there are 14 different equilibrium positions of the minor bodies which evolve in the neighborhood of the Lagrangian equilibrium points of the respective restricted three-body problem with the same value of the reduced mass μ. More precisely, two equilibrium solutions evolve in the neighborhood of each collinear Lagrangian point and on both sides of it. Whipple called these solutions collinear, adopting the terminology used in the restricted three-body

problem. We hereafter denote them with $(S_{1,L_i}{}^{12}, S_{2,L_i}{}^{12})$ and $(S_{1,L_i}{}^{21}, S_{2,L_i}{}^{21})$, $i = 1, 2, 3$. The first index denotes the particular minor body while the second one depicts the respective collinear Lagrangian point L_i, around which the equilibria of the minor bodies evolve. The double upper index used in this section (e.g., ^{12}) describes the relative position of the minor bodies with respect to the Lagrangian point. For example, when body S_1 is located on the left side of the Lagrangian point and body S_2 on the right one, then the upper double index is (^{12}). In the opposite case index (^{21}) is used. In the first case the coordinates of the two minor bodies satisfy the inequality $x_{1,L_i}{}^{12} < x_{L_i} < x_{2,L_i}{}^{12}$ while in the second one, they satisfy the relation $x_{2,L_i}{}^{21} < x_{L_i} < x_{1,L_i}{}^{21}$. Furthermore, four equilibrium solutions exist near a triangular Lagrangian point L_i $(\mu - 0.5, \pm\sqrt{3}/2)$, $i = 4, 5$, where the plus sign stands for L_4 and the minus for L_5. Whipple also stated that two of these solutions lie on a straight line which connects the triangular Lagrangian point with the origin (*inline* equilibria). However, by making more precise calculations we have found that this line does not pass through the origin O but forms a small angle φ with the direction OL_4 (or OL_5). The remaining two equilibrium solutions are located on a line which is perpendicular to the previous one and crosses it at the triangular Lagrangian point. For this reason, they are called *perpendicular*. By using the same notation rules as before, we symbolize the inline and the perpendicular equilibria as $(S_{1,\mathrm{INL}_i}{}^{jk}, S_{2,\mathrm{INL}_i}{}^{jk})$ and $(S_{1,\mathrm{PERL}_i}{}^{jk}, S_{2,\mathrm{PERL}_i}{}^{jk})$, $i = 4, 5$, $j, k = 1, 2$, $j \neq k$, respectively. Here we note that the equilibrium positions have been calculated by Whipple [1], under the approximated assumption that the center of mass of the minor bodies in an equilibrium configuration almost coincides with the corresponding Lagrangian point of the restricted three-body problem. This means that the coordinates $(x_{1e}, y_{1e}, x_{2e}, y_{2e})$ of the minor bodies in an equilibrium position approximately satisfy the relations

$$\begin{aligned} \mu_1 x_{1e} + \mu_2 x_{2e} &= (\mu_1 + \mu_2)\, x_{L_i}, \\ \mu_1 y_{1e} + \mu_2 y_{2e} &= (\mu_1 + \mu_2)\, y_{L_i}. \end{aligned} \tag{6}$$

We have made all the computations from scratch by considering the four coordinates of the minor bodies as independent variables, and we have adjusted the numerical methods used to a new and more general treatment of the problem. Obviously, this results in more complex and extended expressions as well. Further details will be given in a later section of this paper. Figure 2 shows the Lagrangian equilibrium positions of the restricted three-body problem, while Figures 3 and 4 are magnifications of the dotted small frames of Figure 2 showing the distribution of the equilibrium positions of the minor bodies in the neighborhood of the collinear Lagrangian points (Figure 3) and of the triangular L_4 one (Figure 4), for the two considered cases. Tables 1 and 2 contain the numerical results which concern the two considered cases, while Tables 3 and 4 contain the values of the Lagrangian points of the respective restricted three-body systems. In Table 5 we give the dimensionless and the physical values of the distances between the minor bodies (their data are given in Appendices A and B) in a pair of equilibria in the Sun-Jupiter-binary asteroids and the Earth-Moon-dual satellites systems.

3.2. Parametric Variation of the Equilibrium States. In this section we investigate the parametric dependence of the equilibrium positions of the two minor bodies which were calculated in the previous paragraph. Obviously, when the two minor masses are equal, then $(S_{1e}, S_{2e}) \equiv (S_{2e}, S_{1e})$. Otherwise, the distance of the heavier minor body from L_i is smaller than the one from its companion. The obtained results are depicted in Figures 5 and 6. Without loss of generality and for comparison reasons, we have considered equal masses of the minor bodies, $\mu_1 = \mu_2$. In any other case, we obtain similar results, provided that the size of both masses is of the same order. Figure 5 shows the variation of the equilibrium positions with μ when $\mu_1 = \mu_2 = 10^{-12}$. We symbolize with dist $= (L_i S_{1,L_i}{}^{jk})$, $i = 1, \ldots, 5$, $j, k = 1, 2$, $j \neq k$ the distances of the equilibrium location of a minor body S_1 (or S_2) from its neighboring Lagrangian point L_i. We note that the distances of all the equilibrium positions, except for those of the perpendicular ones, slightly vary for all values of μ in the range $0 < \mu \leq 0.5$. On the contrary, the distances of the perpendicular points from their neighboring triangular Lagrangian ones decrease exponentially with μ. Figure 6 shows the evolution of these curves for three different values of μ_1, μ_2, when $\mu_1 = \mu_2 = 10^{-14}$ (full lines), $\mu_1 = \mu_2 = 10^{-15}$ (dotted lines), and $\mu_1 = \mu_2 = 10^{-16}$ (dashed lines). Such, Figure 6(a) depicts these variations for the collinear equilibrium locations, while Figure 6(b) shows these variations for the "inline" and the "perpendicular" ones. As we see, when μ_1, μ_2 decrease, the respective curves are displaced towards the lower part of the diagram. In other words, when the minor bodies become lighter, their distances from the Lagrangian points decrease as well (they approach the Lagrangian points). We additionally observe an accumulation of these curves as the two masses μ_1, μ_2 decrease.

As we have already mentioned, the inline solutions are located on a straight line which forms a small angle φ with the line OL_i which connects the triangular Lagrangian point L_i, $i = 4, 5$, with the origin O. Figure 7(a) shows an exaggerated sketch of the inline and perpendicular locations. With ω, θ we symbolize the angles between the x-axis and OL_4 and the straight line formed by the two inline points, respectively.

In Figure 7(b) we have drawn the variation of the slopes λ of the two straight lines, OL_4 (blue curve) and the line passing through the two inline equilibria (red curve), when $\mu \in [0.01, 0.49]$ and the masses of the two minor bodies are equal, $\mu_1 = \mu_2 = 10^{-12}$. We see that for very small values of μ the two curves almost coincide. This means that their slopes are almost equal. As μ increases the declination angle φ increases as well, and the two curves of the diagram go away from each other, until μ tends to the limit value $\mu = 0.5$ where the slopes of both curves tend to infinity ($\mu \to 0.5$, inline $\to$

Table 1: Sun-Jupiter-binary asteroids (case A).

(a) Collinear equilibrium solutions $(S_{1,L_i}{}^{jk}, S_{2,L_i}{}^{jk})$, $i = 1, 2, 3$ $j, k = 1, 2$ $j \neq k$.

	$x_{1,L_i}{}^{jk}$	$y_{1,L_i}{}^{jk}$	$x_{2,L_i}{}^{jk}$	$y_{2,L_i}{}^{jk}$	Jacobian constant C (10^{-15})	Stability
$(S_{1,L_1}{}^{12}, S_{2,L_1}{}^{12})$	−1.06883 15127	0	−1.06882 65629	0	3.037482	U
$(S_{1L_1}{}^{21}, S_{2,L_1}{}^{21})$	−1.06882 95327	0	−1.06883 44827	0	3.037482	U
$(S_{1,L_2}{}^{12}, S_{2,L_2}{}^{12})$	−0.93236 65174	0	−0.93236 18589	0	3.038764	U
$(S_{1,L_2}{}^{21}, S_{2,L_2}{}^{21})$	−0.93236 46541	0	−0.93236 93124	0	3.038764	U
$(S_{1,L_3}{}^{12}, S_{2,L_3}{}^{12})$	1.00039 60615	0	1.00040 29939	0	3.000966	U
$(S_{1,L_3}{}^{21}, S_{2,L_3}{}^{21})$	1.00039 88345	0	1.00039 19022	0	3.000966	U

(b) Inline $(S_{1,\mathrm{INL}_i}{}^{jk}, S_{2,\mathrm{INL}_i}{}^{jk})$ and perpendicular $(S_{1,\mathrm{PERL}_i}{}^{jk}, S_{2,\mathrm{PERL}_i}{}^{jk})$ equilibrium solutions, $i = 4, 5$, $j, k = 1, 2$ $j \neq k$

	$x_{1,\mathrm{INL}_i}{}^{jk}$	$y_{1,\mathrm{INL}_i}{}^{jk}$	$x_{2,\mathrm{INL}_i}{}^{jk}$	$y_{2,\mathrm{INL}_i}{}^{jk}$	Jacobian constant C (10^{-15})	Stability
$(S_{1,\mathrm{INL}_4}{}^{12}, S_{2,\mathrm{INL}_4}{}^{12})$	−0.49904 68176	0.86602 66052	−0.49904 33524	0.86602 05977	2.999844	U
$(S_{1,\mathrm{INL}_4}{}^{21}, S_{2,\mathrm{INL}_4}{}^{21})$	−0.49904 54315	0.86602 42022	−0.49904 88967	0.86603 02098	2.999844	U
$(S_{1,\mathrm{INL}_5}{}^{12}, S_{2,\mathrm{INL}_5}{}^{12})$	−0.49904 68176	−0.86602 66052	−0.49904 33524	−0.86602 05977	2.999844	U
$(S_{1,\mathrm{INL}_5}{}^{21}, S_{2,\mathrm{INL}_5}{}^{21})$	−0.49904 54315	−0.86602 42022	−0.49904 88967	−0.86603 02098	2.999844	U
	$x_{1,\mathrm{PERL}_i}{}^{jk}$	$y_{1,\mathrm{PERL}_i}{}^{jk}$	$x_{2,\mathrm{PERL}_i}{}^{jk}$	$y_{2,\mathrm{PERL}_i}{}^{jk}$	Jacobian constant C (10^{-15})	Stability
$(S_{1,\mathrm{PERL}_4}{}^{12}, S_{2,\mathrm{PERL}_4}{}^{12})$	−0.49905 95557	0.86601 76565	−0.49899 23934	0.86605 63936	2.999844	S
$(S_{1,\mathrm{PERL}_4}{}^{21}, S_{2,\mathrm{PERL}_4}{}^{21})$	−0.49903 26917	0.86603 31517	−0.49909 98494	0.86599 44131	2.999844	S
$(S_{1,\mathrm{PERL}_5}{}^{12}, S_{2,\mathrm{PERL}_5}{}^{12})$	−0.49905 95557	−0.86601 76565	−0.49899 23934	−0.86605 63936	2.999844	S
$(S_{1,\mathrm{PERL}_5}{}^{21}, S_{2,\mathrm{PERL}_5}{}^{21})$	−0.49903 26917	−0.86603 31517	−0.49909 98494	−0.86599 44131	2.999844	S

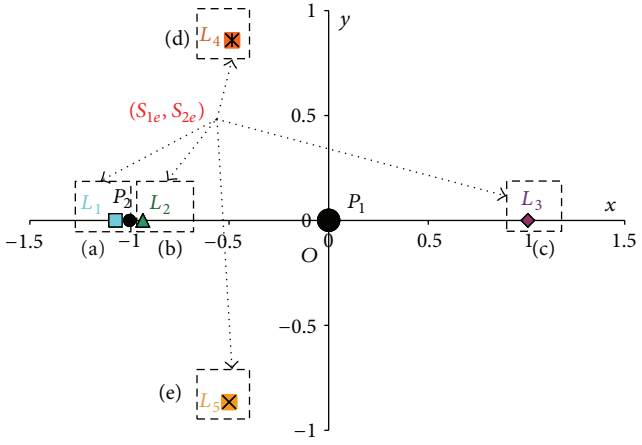

Figure 2: The equilibrium solutions (S_{1e}, S_{2e}) of the minor bodies in the 2+2 body problem are located inside the dotted frames and very close to the Lagrangian points, the distribution of which corresponds to $\mu = 0.0009538754$. We mark these frames with (a), (b), (c), (d), and (e).

OL_4, $\lambda_{\mathrm{inline}} \to \lambda_{OL_4}$, $\omega = 90^\circ$). Figures 7(c) and 7(d) show an alternative way of this variation.

In Figure 7(c) we show the values of the angle of declination φ (red points) calculated for various values of the reduced mass μ. The continuous blue line is the approximated curve obtained by means of a fourth degree polynomial. By testing various coefficients, we have found that the best fitting curve (blue) is achieved when

$$\phi(\mu) = 22.9594\mu + 17.9969\mu^2 - 193.986\mu^3 + 130.327\mu^4. \quad (7)$$

Figure 7(d) shows the directions of the inline equilibrium pairs for three particular values of μ.

(1) If $\mu \to 0$, then $P_1 \to O\,(0, 0)$, $P_2 \to (-1, 0)$, $L_4 \to (-0.5, y_{L_4})$, $\varphi \to 0^\circ$, and the direction of the inline equilibria coincides with the line OL_4 (green color).

(2) If $\mu = 0.5$ (Copenhagen case [12]), then P_1 (0.5, 0), P_2 (−0.5, 0), the triangular L_4 lies on the y-axis, $\varphi \to 0^\circ$, and inline $\equiv OL_4$ (red color).

(3) If $\mu = 0.25$, then P_1 (0.25, 0), P_2 (−0.75, 0), the coordinates of the triangular L_4 are $(-0.25, y_{L_4})$, and φ takes its maximum value $\varphi_{\max} \cong 4.4^\circ$ (blue color).

3.3. Stability. Whipple proved that the collinear and inline triangular solutions are unstable for every value of the mass parameters. However, for some values of these parameters, the perpendicular solutions are stable (see Tables 1 and 2 and Figure 8). In these tables the letter U stands for unstable and the letter S for stable. In the diagram of Figure 8 (Whipple [1]), the horizontal axis counts the quantity $\mu' = \mu_2/(\mu_1 + \mu_2)$, and as we can see, the limit curve which separates the two regions of stability and instability decreases exponentially

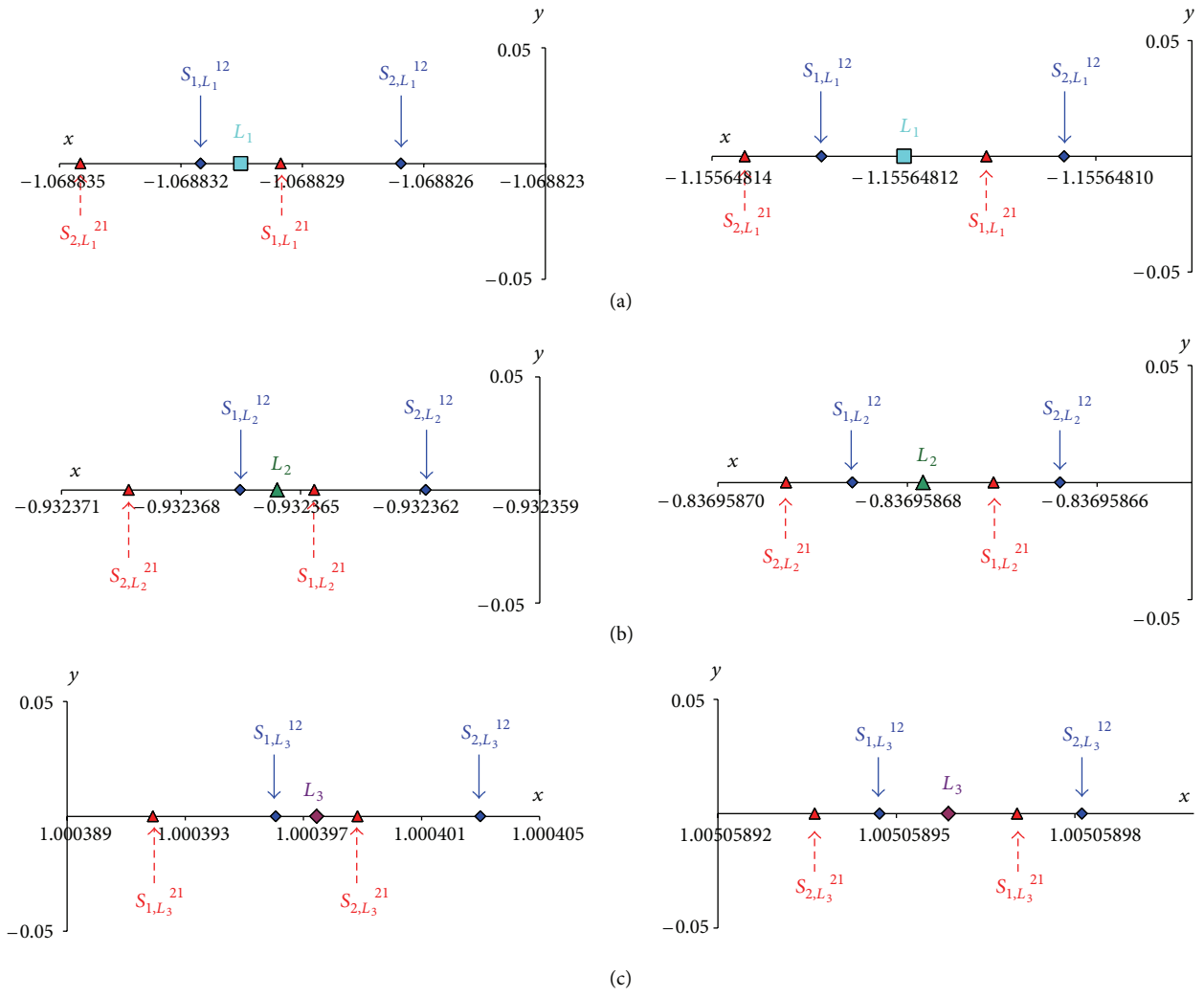

FIGURE 3: Distribution of the collinear equilibrium solutions in the neighborhood of L_1 (a), L_2 (b), and L_3 (c) Lagrangian points. $(S_{1,L_i}{}^{12}, S_{2,L_i}{}^{12})$ (in blue) and $(S_{1,L_i}{}^{21}, S_{2,L_i}{}^{21})$ (in red), $i = 1, 2, 3$, for two different cases; (A) Sun-Jupiter-binary asteroids, (B) Earth-Moon-dual satellites.

as μ decreases. The two considered cases are depicted in the diagram with the points A and B and both lie in the stable area of the diagram.

4. Structure and Parametric Evolution of the Attracting Regions for Systems with Two or Four Degrees of Freedom

As we have mentioned before, the exact locations of the equilibria of the system are found numerically with the use of an iterative scheme. In everyday practice, the process starts when an initial approximation is given and stops when an equilibrium solution is found with a predetermined accuracy. We have used the well-known Newton-Raphson method since it is a fast (it converges quadratically), simple, and accurate computational tool. For comparison reasons, we also have investigated the attracting regions of both the restricted three-body problem which is characterized by two degrees of freedom and the restricted 2+2-body problem with four degrees of freedom. Here we note that we have obtained similar results by using various numerical methods and that the whole process aims to locate the initial values that lead to a particular equilibrium state in the fastest possible way, thus saving computing time.

4.1. General Concept for a System with Two Degrees of Freedom: Attracting Regions in the Planar Restricted Three-Body Problem. By considering systems with two degrees of freedom (x, y) and assuming that equilibrium points exist on the xy-plane, the initial approximation is a point (x_0, y_0) on this plane, and the successive iterations of the algorithm form a crooked path starting at (x_0, y_0) and ending at (x_L, y_L) (if of course the algorithm converges for these initial values). This may happen for several different initial approximations, and usually, we are able to find those which lead to a particular

Table 2: Earth-Moon-dual satellite system (case B).

(a) Collinear equilibrium solutions $(S_{1,L_i}{}^{jk}, S_{2,L_i}{}^{jk})$, $i = 1, 2, 3$ $j, k = 1, 2$ $j \neq k$.

	$x_{1,L_i}{}^{jk}$	$y_{1,L_i}{}^{jk}$	$x_{2,L_i}{}^{jk}$	$y_{2,L_i}{}^{jk}$	Jacobian constant C (10^{-20})	Stability
$(S_{1,L_1}{}^{12}, S_{2,L_1}{}^{12})$	−1.15564 81286	0	−1.15564 81033	0	3.772852	U
$(S_{1L_1}{}^{21}, S_{2,L_1}{}^{21})$	−1.15564 81114	0	−1.15564 81366	0	3.772852	U
$(S_{1,L_2}{}^{12}, S_{2,L_2}{}^{12})$	−0.83695 86858	0	−0.83695 86639	0	3.792084	U
$(S_{1,L_2}{}^{21}, S_{2,L_2}{}^{21})$	−0.83695 86709	0	−0.83695 86928	0	3.792084	U
$(S_{1,L_3}{}^{12}, S_{2,L_3}{}^{12})$	1.00505 89472	0	1.00505 89812	0	3.582608	U
$(S_{1,L_3}{}^{21}, S_{2,L_3}{}^{21})$	1.00505 89703	0	1.00505 89363	0	3.582608	U

(b) Inline $(S_{1,\mathrm{INL}_i}{}^{jk}, S_{2,\mathrm{INL}_i}{}^{jk})$ and perpendicular $(S_{1,\mathrm{PERL}_i}{}^{jk}, S_{2,\mathrm{PERL}_i}{}^{jk})$ equilibrium solutions, $i = 4, 5$, $j, k = 1, 2$ $j \neq k$

	$x_{1,\mathrm{INL}_i}{}^{jk}$	$y_{1,\mathrm{INL}_i}{}^{jk}$	$x_{2,\mathrm{INL}_i}{}^{jk}$	$y_{2,\mathrm{INL}_i}{}^{jk}$	Jacobian constant C (10^{-20})	Stability
$(S_{1,\mathrm{INL}_4}{}^{12}, S_{2,\mathrm{INL}_4}{}^{12})$	−0.48785 82696	0.86602 54139	−0.48785 82526	0.86602 53842	3.553904	U
$(S_{1,\mathrm{INL}_4}{}^{21}, S_{2,\mathrm{INL}_4}{}^{21})$	−0.48785 82580	0.86602 53937	−0.48785 82749	0.86602 54234	3.553904	U
$(S_{1,\mathrm{INL}_5}{}^{12}, S_{2,\mathrm{INL}_5}{}^{12})$	−0.48785 82696	−0.86602 54139	−0.48785 82526	−0.86602 53842	3.553904	U
$(S_{1,\mathrm{INL}_5}{}^{21}, S_{2,\mathrm{INL}_5}{}^{21})$	−0.48785 82580	−0.86602 53937	−0.48785 82749	−0.86602 54234	3.553904	U
	$x_{1,\mathrm{PERL}_i}{}^{jk}$	$y_{1,\mathrm{PERL}_i}{}^{jk}$	$x_{2,\mathrm{PERL}_i}{}^{jk}$	$y_{2,\mathrm{PERL}_i}{}^{jk}$	Jacobian constant C (10^{-20})	Stability
$(S_{1,\mathrm{PERL}_4}{}^{12}, S_{2,\mathrm{PERL}_4}{}^{12})$	−0.48785 83121	0.86602 53762	−0.48785 81701	0.86602 54572	3.553904	S
$(S_{1,\mathrm{PERL}_4}{}^{21}, S_{2,\mathrm{PERL}_4}{}^{21})$	−0.48785 82155	0.86602 54313	−0.48785 83575	0.86602 53504	3.553904	S
$(S_{1,\mathrm{PERL}_5}{}^{12}, S_{2,\mathrm{PERL}_5}{}^{12})$	−0.48785 83121	−0.86602 53762	−0.48785 81701	−0.86602 54572	3.553904	S
$(S_{1,\mathrm{PERL}_5}{}^{21}, S_{2,\mathrm{PERL}_5}{}^{21})$	−0.48785 82155	−0.86602 54313	−0.48785 83575	−0.86602 53504	3.553904	S

Table 3: Lagrangian points of the system Sun-Jupiter-point-like mass

L_i	x_{L_i}	y_{L_i}	C: Jacobian constant
L_1	−1.06883 05227 09332	0	3.03844 17168 44306
L_2	−0.93236 55857 74543	0	3.03971 38039 57303
L_3	1.00039 74480 46084	0	3.00190 68218 17403
L_4	−0.49904 61313 20285	0.86602 53998 83256	3.00000 00000 00000
L_5	−0.49904 61313 20285	−0.86602 53998 83256	3.00000 00000 00000

equilibrium position (provided that more than one exists). In other words, an equilibrium point plays the role of a target or that of an "attractor" regardless of its real state of stability, since we can reach it even if we start from different initial values and follow different paths of successive approximating steps.

All the initial points that lead to the same equilibrium point form a set of points which constitutes the so-called attracting region or attracting domain of this equilibrium point (Croustalloudi and Kalvouridis [13, 14]). Consequently, there are as many attracting regions as the number of the equilibrium points. For instance, in the restricted three-body problem there are five such regions and so on (Figure 9(a)). We symbolize these areas with $R(L_i)$, where L_i, $i = 1, 2, \ldots, 5$ are the equilibrium points. In practice, we determine these regions by applying a double scanning of the (x, y) plane in a predetermined area of it ($-2.5 \leq x_0, y_0 \leq 2.5$) by using a predetermined step (0.01) and a predetermined accuracy (let us say 10^{-12}). This means that we have checked 250,000 initial values. Whatever the numerical method is, the structure of the attracting regions shows all the symmetry characteristics of the dynamical system as well as some aspects of the nonlinearity of the problem. Each attracting region generally consists of some smaller regions, all the points of which lead to a particular equilibrium point. We call these areas "compact" and they have a deterministic character, since small changes in the initial values lead to the same equilibrium solution. However, their boundaries are neither simple nor well-defined lines and are characterized by rather entangled and complex structures which frame the "compact" area. Apart from these areas, there are also many dispersed points which are generally mixed with the dispersed points of other similar regions. In this case a small change in the initial values may lead to a different target-equilibrium position. This sensitivity shows a chaotic behavior, since the prediction of the final

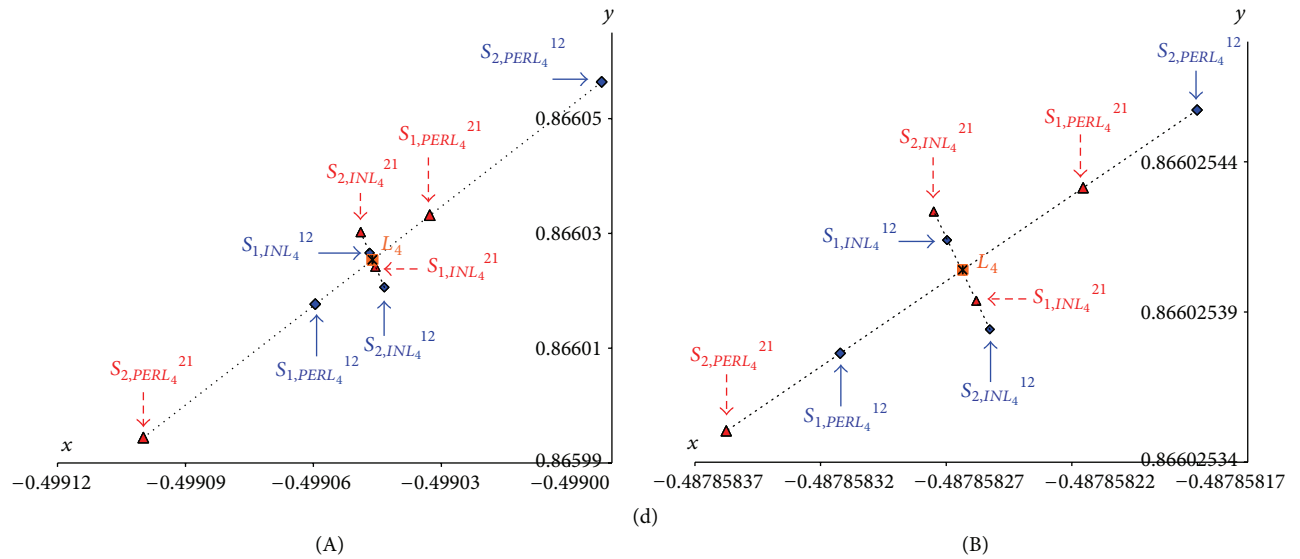

(d)

FIGURE 4: Distribution of the pairs of the inline and perpendicular equilibria in the neighbourhood of the triangular Lagrangian point L_4 for three different cases; (A) Sun-Jupiter-binary asteroids, (B) Earth-Moon-dual satellites.

TABLE 4: Lagrangian points of the system Earth-Moon-point-like mass.

L_i	x_{L_i}	y_{L_i}	C: Jacobian constant
L_1	−1.15564 81199 75768	0	3.18408 49162 90530
L_2	−0.83695 86783 47250	0	3.20025 38143 78359
L_3	1.00505 89587 71169	0	3.02413 26209 77968
L_4	−0.48785 82634 14611	0.86602 54040 12551	3.00000 00000 00000
L_5	−0.48785 82634 14611	−0.86602 54040 12551	3.00000 00000 00000

target is not possible. Furthermore, the coexistence of many "attractors" causes the creation of a fractal structure of the basin boundaries (Peitgen et al. [15]).

The equations of motion which describe the two-dimensional motion of a point-like small mass on the xy-plane of a synodic reference frame are

$$\ddot{x} - 2\dot{y} = \frac{\partial U}{\partial x} = U_x,$$
$$\ddot{y} + 2\dot{x} = \frac{\partial U}{\partial y} = U_y, \tag{8}$$

where

$$U = \frac{1}{2}\left(x^2 + y^2\right) + \frac{1-\mu}{r_1} + \frac{\mu}{r_2} + \frac{1}{2}\mu(1-\mu) \tag{9}$$

is the potential function and

$$r_1^2 = (x-\mu)^2 + y^2, \qquad r_2^2 = (x-\mu+1)^2 + y^2 \tag{10}$$

are the distances of the particle from the primaries. We have studied the attracting regions for many values of parameter μ, and here we have considered the case that corresponds to the Sun-Jupiter-asteroid system ($\mu = 0.0009538754$). Figure 9(a) shows the attracting regions of the three collinear L_1, L_2, L_3 and the triangular L_4 (the second triangular point L_5 is symmetric with respect to the x-axis) Lagrangian points. The bar chart of Figure 9(b) gives the number of points of each attracting region as the percentage of the total number of tested points for the same system.

Our conclusions regarding this problem can be summarized as follows.

(1) The attracting region $R(L_1)$ occupies the smallest area of all the basins for every value of μ in the range of $0 < \mu \leq 0.5$. It consists of two small "compact" areas, which develop on the left of primary P_2 and of the dispersed points (Figure 9(a) (red)). As μ increases, region $R(L_1)$ expands, while the "compact" one widens, and the dispersed points increase and become denser around the "compact" areas.

(2) The attracting region $R(L_2)$ consists of two "compact" areas (Figure 9(a) (yellow)). The first one extends between the two primaries P_1 and P_2, while the second one is extended beyond the "compact" regions of $R(L_1)$. The dispersed points of this basin, as we have already mentioned, form fractal boundaries. As μ

Table 5: Distances between the minor bodies in a pair of equilibria in the Sun-Jupiter-binary asteroids and the Earth-Moon-dual satellites systems.

Equil.states	Sun-Jupiter-binary asteroids Distances between S_{1e}, S_{2e}		Earth-Moon-dual satellites Distances between S_{1e}, S_{2e}	
(S_{1e}, S_{2e})	Dimensionless	Physical (Km)	Dimensionless	Physical (m)
$(S_{1,L_1}{}^{12}, S_{2,L_1}{}^{12})$	$4.94 \cdot 10^{-6}$	3 850.548	$2.53 \cdot 10^{-8}$	9.72
$(S_{1,L_2}{}^{12}, S_{2,L_2}{}^{12})$	$4.65 \cdot 10^{-6}$	3 623.940	$2.19 \cdot 10^{-8}$	8.41
$(S_{1,L_3}{}^{12}, S_{2,L_3}{}^{12})$	$6.93 \cdot 10^{-6}$	5 392.852	$3.4 \cdot 10^{-8}$	13.07
$(S_{1,\mathrm{INL}_4}{}^{12}, S_{2,\mathrm{INL}_4}{}^{12}$	$6.94 \cdot 10^{-6}$	5 395.030	$3.42 \cdot 10^{-8}$	13.15
$(S_{1,\mathrm{PERL}_4}{}^{12}, S_{2,\mathrm{PERL}_4}{}^{12})$	$7.75 \cdot 10^{-5}$	60 314.315	$1.63 \cdot 10^{-7}$	62.84

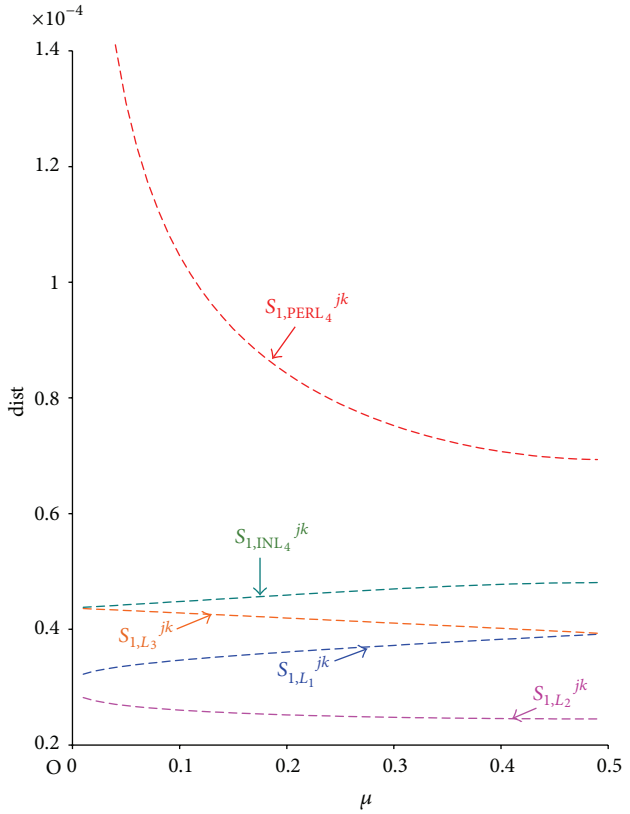

Figure 5: Variation of the distances (dist) of the equilibrium positions of the minor bodies from their neighboring Lagrangian points L_i, with mass parameter μ ($\mu_1 = \mu_2 = 10^{-12}$).

augments, the number of the points in $R(L_2)$ increases as well; at the same time, the dispersed points become denser, thus forming fractal protrusions.

(3) Attracting region $R(L_3)$ is homothetic of $R(L_1)$. The homothetic ratio and the homothetic center can be easily calculated for every value of mass parameter μ. As μ increases ($0 < \mu \leq 0.5$), this ratio approaches 1 while the homothetic center approaches equilibrium position L_2. Region $R(L_3)$ consists of two "compact" areas which extend on the right of primary P_1, as well as the numerous dispersed points (Figure 9(a) (light blue)).

(4) Attracting region $R(L_4)$ consists of several "compact" areas which extend on the semiplane $y > 0$. The dispersed points spread all over the plane. As μ increases, $R(L_4)$ expands, and the "compact" areas tend to unite, thus forming a great "compact" area, while the dispersed points become denser inside the area of the basin boundaries, exactly like the ones in $R(L_2)$ (Figure 9(a) (green)). Attracting region $R(L_5)$ is symmetric with $R(L_4)$ as regards the x-axis and therefore presents the exact same characteristics (Figure 9(a) (dark blue)).

4.2. General Concept for a System with Four Degrees of Freedom; Attracting Regions in the (2 + 2) Body Problem. In this case there are four independent variables (x_1, y_1, x_2, y_2), the equilibrium points are the solutions of the algebraic system $U_{x_1} = U_{y_1} = U_{x_2} = U_{y_2} = 0$, and the Newton-Raphson iterator takes the form

$$x_i^{(n)} = x_i^{(n-1)} - \left.\frac{J_{x_i}}{J}\right|_{x_1^{(n-1)}, y_1^{(n-1)}, x_2^{(n-1)}, y_2^{(n-1)}},$$
$$y_i^{(n)} = y_i^{(n-1)} + \left.\frac{J_{y_i}}{J}\right|_{x_1^{(n-1)}, y_1^{(n-1)}, x_2^{(n-1)}, y_2^{(n-1)}}, \quad i = 1, 2, \tag{11}$$

where

$$J = f\left(U_{x_i x_j}, U_{y_i y_j}, U_{x_i y_j}\right),$$
$$J_{x_k} = f_k\left(U_{x_i}, U_{y_i}, U_{x_i x_j}, U_{y_i y_j}, U_{x_i y_j}\right),$$
$$J_{y_k} = g_k\left(U_{x_i}, U_{y_i}, U_{x_i x_j}, U_{y_i y_j}, U_{x_i y_j}\right), \quad i, j, k = 1, 2. \tag{12}$$

The quantities J, J_{x_k}, J_{y_k} are functions of the first and second partial derivatives of the potential function U (2) with respect to the four variables of the problem. The iterative process starts when a pair of initial approximations $S_{10}(x_{10}, y_{10})$ and $S_{20}(x_{20}, y_{20})$ is given and stops when a pair of equilibrium points $S_{1e}(x_{1e}, y_{1e})$ and $S_{2e}(x_{2e}, y_{2e})$ is found with the predetermined accuracy. Theoretically, in order to obtain the attracting regions of all the equilibrium states we have to apply a quadruple scanning to check the entirety of the initial positions $(x_{10}, y_{10}, x_{20}, y_{20})$. In this case, the obtained geometric forms of the attracting regions

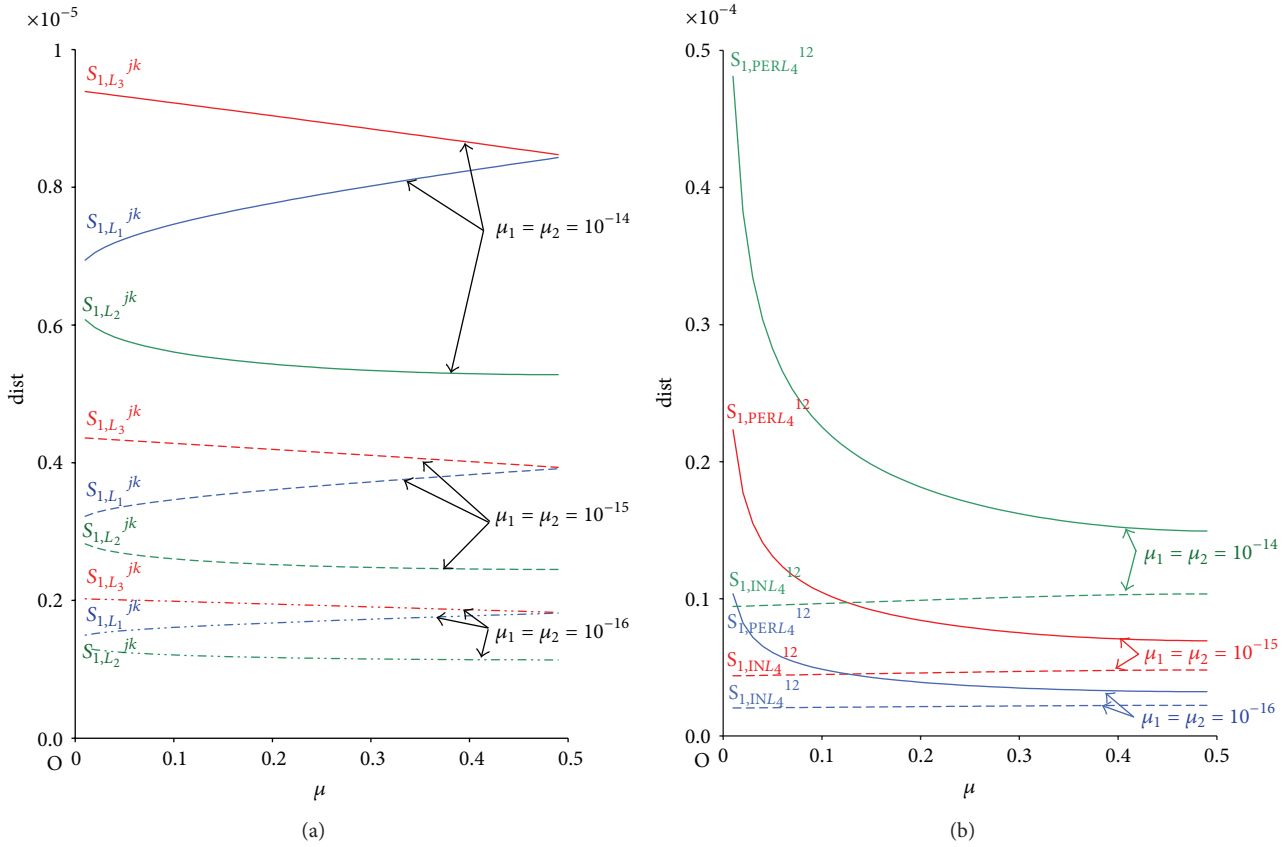

FIGURE 6: Variation of the distances of the equilibrium positions of the minor bodies from their neighboring Lagrangian point with mass parameter μ for the case where the two minor bodies have equal masses. (a) Collinear and (b) triangular solutions.

will be hypersurfaces in the four-dimensional space. Since the construction of such surfaces is not feasible, we have simplified the whole process by considering that the initial position of one of the small bodies, let us say of S_{20}, is known. Then by varying, through a double scanning, the initial pair (x_{10}, y_{10}) of the other body S_1 we obtain the starting values which are necessary for the Newton-Raphson algorithm. If, for a set of initial values, the method converges, the final target will be an equilibrium state S_{1e} and S_{2e} of the minor bodies. This process is repeated until all the values (x_{10}, y_{10}) of the predetermined area of the xy-plane are exhausted.

We have applied the above technique to many different cases of the 2+2 body problem, and hereafter we have considered the results of the Sun-Jupiter-2 asteroids system, where $\mu = 0.0009538754$, $\mu_1 = 8 * 10^{-16}$, and $\mu_2 = 2 * 10^{-16}$. This choice has made for comparison reasons with the results obtained from the Sun-Jupiter-asteroid system.

Here we note that, although the basic idea of the processes as described in the two considered problems is the same, the behavior of the algorithm is quite different. As we have mentioned in the previous section (Section 4.1), almost every initial value (x_0, y_0) in the RTBP can lead to any of the five existing targets-equilibrium points. Therefore, at the end of the double-scanning process, almost 100% of the total initial values converge and five attracting regions are created which correspond to the five Lagrangian points.

However, in the 2+2 BP and for a given initial value S_{20}, most of the initial values (x_{10}, y_{10}) of the scanned area do not lead to convergence, and also all the converging initial values lead to the equilibrium states which evolve in the neighborhood of a single Lagrangian point. Therefore, for each arbitrary value S_{20} there are five different possibilities (as many as the Lagrangian points). This also means that, if for an arbitrary S_{20} the method converges to the equilibrium states around a particular Lagrangian point L_i, for another value S_{20} it may lead to the same or another target; for example, it may terminate to the equilibrium states around L_4, and so forth. At the end of the process (for a given S_{20}), only the attracting regions $R_{S_1}(L_i^e)$ of the equilibrium states e, which evolve in the neighborhood of one Lagrangian point L_i, are formed. Here, we may remind that each attracting region consists of those initial points that converge to a particular equilibrium state of the two minor bodies. So, for each arbitrary value S_{20} the five different possibilities of the converging initial values (x_{10}, y_{10}) can be classified in five sets, which we hereafter call attracting sets. Then, each set consists of the attracting subsets (or attracting regions) of the equilibrium states of the two minor bodies that evolve around a particular Lagrangian

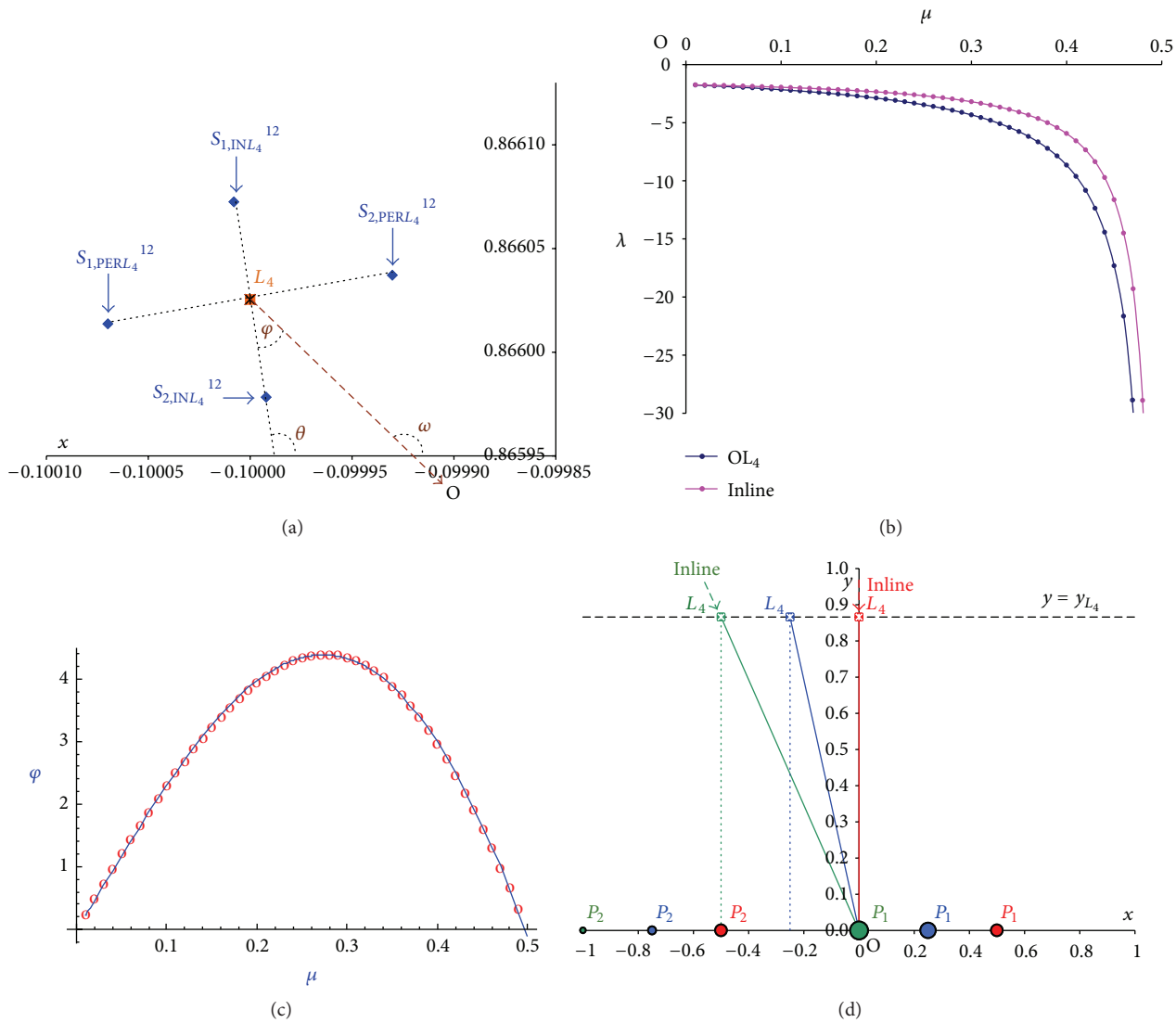

FIGURE 7: (a) The angles ω, θ between the x-axis and OL_4 and the straight line formed by the two inline points, respectively, (b) variation of the slopes λ of the two straight lines, OL_4 (blue curve), and the one passing through the inline equilibria (red curve), with mass parameter μ, (c) angle of declination φ (red points) for various values of μ and the polynomial approximation (blue curve), and (d) directions of the inline equilibrium pairs for three particular values of μ ($\mu \to 0$, and $\mu = 0.25, 0.5$).

point L_i (two equilibrium states for each collinear Lagrangian point and four equilibria for each triangular one) and is symbolized with $R_{S_1}(L_i)$, $i = 1, 2, 3, 4, 5$. In other words, each set which refers to a collinear Lagrangian point is the union of two particular attracting subsets, while each set which refers to a triangular Lagrangian point is the union of four attracting subsets.

Since the initial approximation $S_{20}(x_{20}, y_{20})$ has arbitrarily been selected, we expect that the results obtained by considering different initial values of S_{20} will generally be different. Indeed, this is observed in the attracting subsets, whose size, shape, and internal structure ("compact" areas and dispersed points) depend on the choice of S_{20}. Although the total number of the points remains the same in each attracting set (but differ from one set to the other) for a particular dynamical system, a kind of an "internal exchange or transfer" of points is observed between the attracting subsets of an attracting set when the initial value of S_{20} varies. Figures 10(a)–10(d) show four attracting sets for the considering problem. Three of them, the attracting sets $R_{S_1}(L_i)$, $i = 1, 2, 3$, correspond to the two equilibrium states on both sides of the collinear Lagrangian points L_i, and the $R_{S_1}(L_4)$ corresponds to the four equilibrium states around the triangular point L_4 (the attracting set $R_{S_1}(L_5)$ is symmetric to $R_{S_1}(L_4)$ with respect to the x-axis). In each figure, the attracting subsets are shown with a different color (Figures 10(a)–10(d)). If the colors of the subsets were the same, then we would obtain the attracting sets almost similar to corresponding attracting regions of

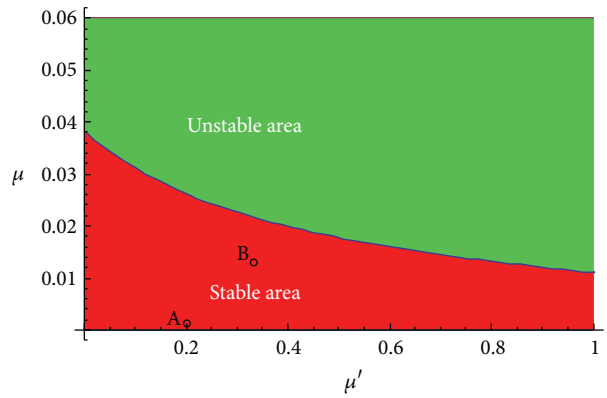

FIGURE 8: Regions of stability (red) and instability (green) for the perpendicular equilibrium points. Points A and B show, respectively, the Sun-Jupiter-binary asteroids system and the Earth-Moon-dual satellites one.

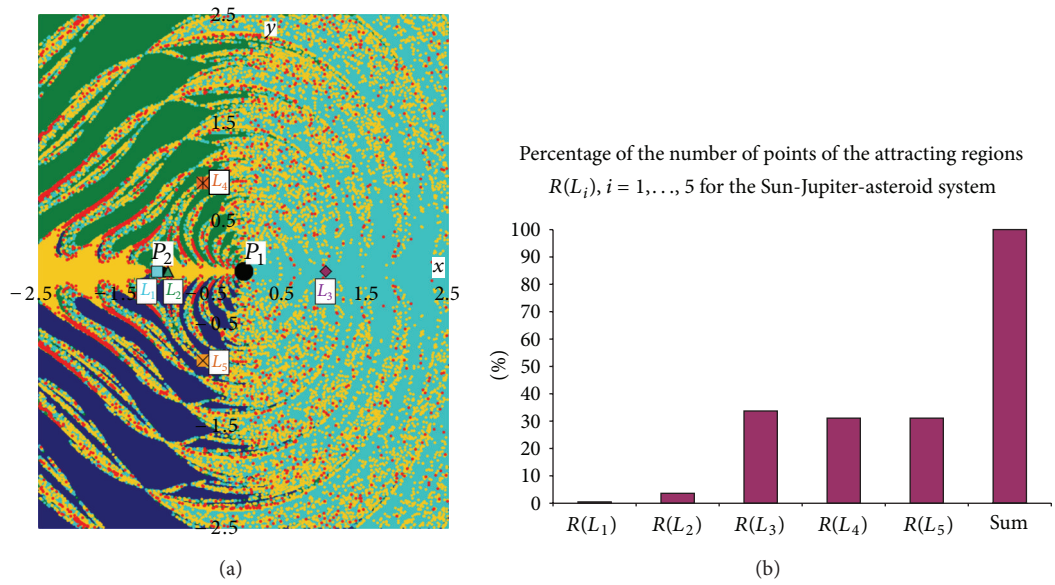

(a) (b)

FIGURE 9: (a) Attracting domains of all Lagrangian points for the Sun-Jupiter-asteroid system: $R(L_1)$ red, $R(L_2)$ yellow, $R(L_3)$ light blue, $R(L_4)$ green, and $R(L_5)$ dark blue color, (b) percent of the number of points of the attracting regions for the same system.

the restricted three-body problem (Figure 9(a)). As we have noted before, however, the arbitrary choice of (x_{20}, y_{20}) does not influence the global characteristics of each set (total number of converging points); nevertheless, it affects the number of the points of each attracting subset. Evidently, the above sets are influenced by the three parameters μ, μ_1, μ_2 of the problem.

Also, it is important to emphasize that, whenever an initial value S_{20} is given, the total number of points (x_{10}, y_{10}) for which the method converges (as a percentage of the total number of the tested points of the plane, which are 250,000) depends on the resultant attracting set and on the three mass parameters. In the bar chart of Figure 11, it is clear that this percentage remains less than 30%, which corresponds to the bigger attracting sets of the considering case.

In what follows we give a short description of the main characteristics of each attracting set $R_{S_1}(L_i)$, $i = 1, \ldots, 5$, as well as their parametric evolution.

4.2.1. The Attracting Set $R_{S_1}(L_1)$. As we have mentioned before, the set $R_{S_1}(L_1)$ consists of two subsets, namely, the attracting subsets $R_{S_1}({L_1}^{12})$ and $R_{S_1}({L_1}^{21})$, which correspond to the two equilibrium states that appear in the neighborhood of the Lagrangian point L_1. $R_{S_1}(L_1)$ is the smallest and poorest attracting set among all the others. Where μ is very small, it consists of tiny "compact" areas and of, rarely found, dispersed points. (Figure 10(a) and incorporated picture). However, when μ increases, this domain expands slightly. Furthermore, the numerous tiny "compact" areas as well as

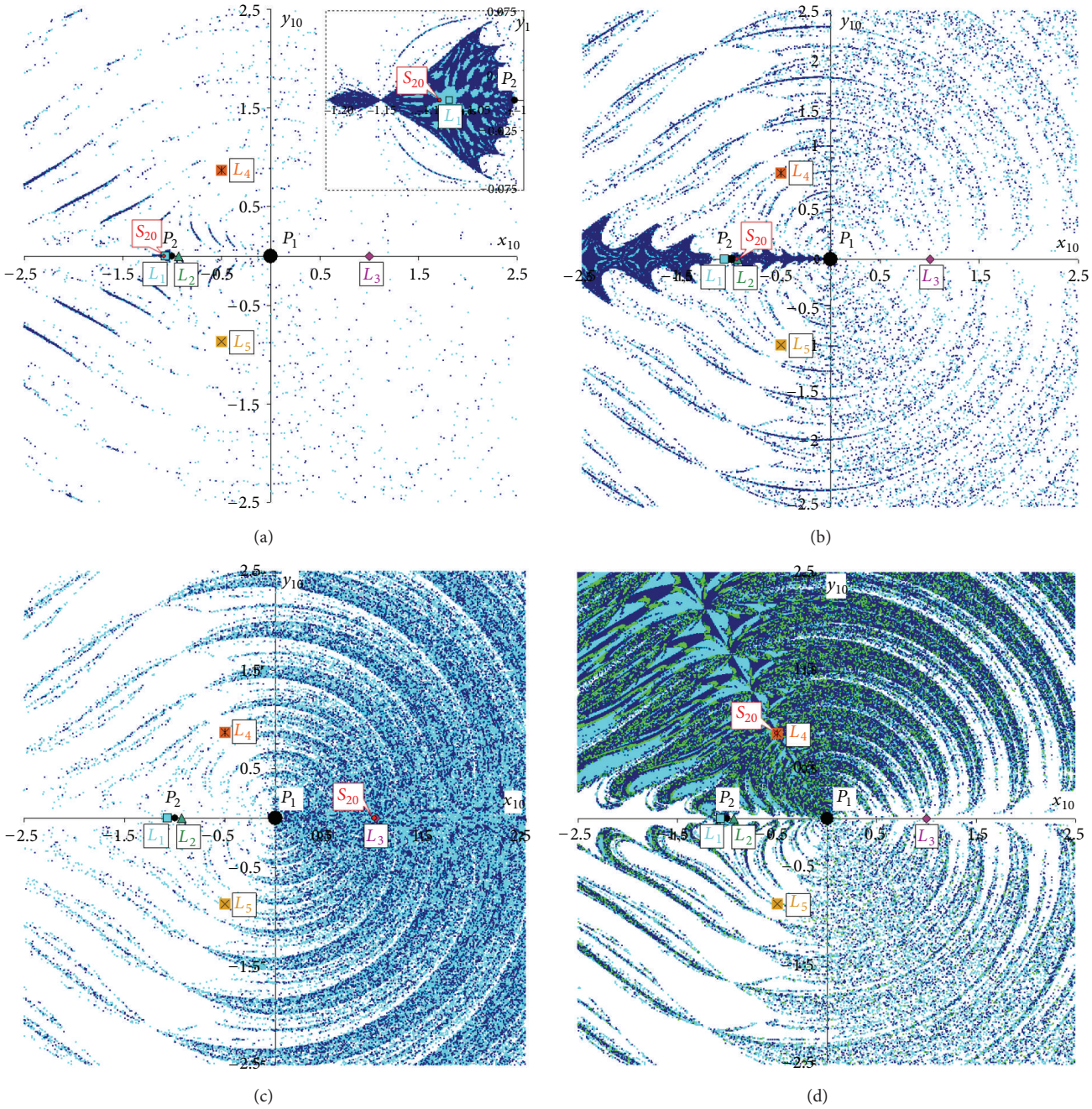

FIGURE 10: Attracting sets (a) $R_{S_1}(L_1)$, (b) $R_{S_1}(L_2)$, (c) $R_{S_1}(L_3)$, and (d) $R_{S_1}(L_4)$ for the Sun-Jupiter-binary asteroids system. Attracting subsets $R_{S_1}(L_i{}^{12})$ (blue), $R_{S_1}(L_i{}^{21})$ (dark blue), $i = 1, 2, 3$ and subsets $R_{S_1}(L_{4,\mathrm{IN}}{}^{12})$ (green), $R_{S_1}(L_{4,\mathrm{IN}}{}^{21})$ (dark green), $R_{S_1}(L_{4,\mathrm{PER}}{}^{12})$ (sky blue), $R_{S_1}(L_{4,\mathrm{PER}}{}^{21})$ (dark blue).

some of the dispersed points are united so as to create a formation which resembles the respective attracting region $R(L_1)$ of the RTBP (Figure 9(a) (red)) but without the same "compactness". All the described changes and the percentages of the converging points are also depicted in the bar chart diagrams of Figures 9(b) and 11.

4.2.2. The Attracting Set $R_{S_1}(L_2)$. This set consists of two subsets, namely, the attracting subsets $R_{S_1}(L_2{}^{12})$ and $R_{S_1}(L_2{}^{21})$, which correspond to the two equilibrium states that evolve around the collinear Lagrangian point L_2. The subsets are characterized by many small "compact" areas and dispersed points. The superposition of the subsets of $R_{S_1}(L_2)$ almost

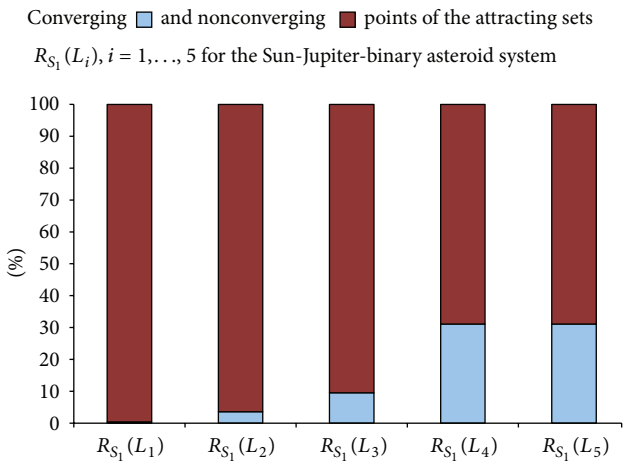

Figure 11: Bar chart with the percentages of the converging and nonconverging points for the Sun-Jupiter-binary asteroids system.

gives the attracting region $R(L_2)$ of the RTBP (Figure 9(a) (yellow), 9(b), 10(b), and 11). As μ varies, the content of the set varies accordingly too.

4.2.3. The Attracting Set $R_{S_1}(L_3)$. It results from the union of the attracting subsets $R_{S_1}({L_3}^{12})$ and $R_{S_1}({L_3}^{21})$, which correspond to the two equilibrium states that appear in the neighborhood of the Lagrangian point L_3 and is homothetic to $R_{S_1}(L_1)$ (Figure 10(c)). The most important aspect is that the total number of points of the whole set (9.5%) is much less than the number of the corresponding set of the RTBP (33.7%), as is clear of a comparison of the respective bar charts of Figures 9(b) and 11.

4.2.4. The Attracting Set $R_{S_1}(L_4)$. It consists of four attracting subsets. Two of them, $R_{S_1}({L_{4,\mathrm{IN}}}^{12})$, $R_{S_1}({L_{4,\mathrm{IN}}}^{21})$, refer to the two inline pairs of equilibrium states and the other two, $R_{S_1}({L_{4,\mathrm{PER}}}^{12})$, $R_{S_1}({L_{4,\mathrm{PER}}}^{21})$, refer to the two perpendicular pairs of equilibrium states that evolve around the triangular Lagrangian point L_4 (Figure 10(d)). Attracting set $R_{S_1}(L_4)$ concentrates the majority of the converging points, that is, approximately 31.1% for the considering problem of the total initial values, which are almost the same with the respective ones of the RTBP (Figures 9(b) and 11). Also, we have observed that when the initial value S_{20} is taken close to L_4, these regions present a complex fractal structure which mainly evolves between the primaries and the equilibrium positions.

Here we note that, if instead of keeping S_{20} constant throughout the scanning process, we shall consider the initial position S_{10} constant, then the patterns of the attracting sets $R_{S_1}(L_i)$ (for a given S_{20}) and of the respective sets $R_{S_2}(L_i)$ (for a given S_{10}) are quite the same. However, there is an internal mutual interchange of the points between the attracting subsets corresponding to the two equilibrium states evolving from both sides of the Lagrangian point L_i. As a consequence, the points which previously belonged to $R_{S_1}({L_i}^{kj})$ are now located in $R_{S_2}({L_i}^{jk})$ and vice versa.

As an example, we present in Figures 12(a) and 12(b) the attracting subsets of the inline and the perpendicular equilibria which evolve in the neighborhood of the Lagrangian point L_4 for the case of Sun-Jupiter-binary asteroids. In each figure we use different colors to show the attracting subsets of the four equilibrium states; light green for $R_{S_1}({L_{4,\mathrm{IN}}}^{12})$ and $R_{S_2}({L_{4,\mathrm{IN}}}^{12})$, green for $R_{S_1}({L_{4,\mathrm{IN}}}^{21})$ and $R_{S_2}({L_{4,\mathrm{IN}}}^{21})$, light blue for $R_{S_1}({L_{4,\mathrm{PER}}}^{12})$ and $R_{S_2}({L_{4,\mathrm{PER}}}^{12})$, blue for $R_{S_1}({L_{4,\mathrm{PER}}}^{21})$ and $R_{S_2}({L_{4,\mathrm{PER}}}^{21})$. By comparing these figures we can confirm that the general patterns remain the same, although there are differences in the interior of the two attracting sets which arise from the fact that a redistribution of the converging points occurs. So, a mutual interchange is observed between the two attracting subsets corresponding to the inline equilibrium states and between the two remaining others corresponding to the perpendicular equilibrium states. Therefore, we observe that $R_{S_1}({L_{4,\mathrm{IN}}}^{12}) \equiv R_{S_2}({L_{4,\mathrm{IN}}}^{21})$, $R_{S_1}({L_{4,\mathrm{IN}}}^{21}) \equiv R_{S_2}({L_{4,\mathrm{IN}}}^{12})$, $R_{S_1}({L_{4,\mathrm{PER}}}^{12}) \equiv R_{S_2}({L_{4,\mathrm{PER}}}^{21})$, and $R_{S_1}({L_{4,\mathrm{PER}}}^{21}) \equiv R_{S_2}({L_{4,\mathrm{PER}}}^{12})$. This finding is also verified in the bar chart of Figure 13 where we have plotted the data of the considered case.

5. Conclusions and Remarks

We have elaborated anew on the problem proposed by Whipple, by following a more general approach and by applying it to two problem cases: (i) the Sun-Jupiter-binary asteroids system and (ii) the Earth-Moon-dual satellites system. We have numerically studied the parametric variation of the equilibrium states, as well as the formation, the structure, and the parametric dependence of the attracting regions of these equilibrium states. Our comments, conclusions, and remarks can be classified into three parts. The first part includes the general remarks which concern the efficiency of the numerical algorithm when applied to both problems: the 2+2 BP (four degrees of freedom) and the RTBP (two degrees of freedom). A second part includes the conclusions concerning the location and the parametric variation of the equilibrium states of the two minor bodies S_1 and S_2. Finally, the third part comprises the conclusions concerning the attracting regions and their evolution, as well as their similarities and their differences as they result from the application to the two aforementioned problems.

(I) Comments Concerning the Efficiency of the Numerical Method. The number of the initial values for which the method converges in the 2+2 BP problem, as a fraction of the total number of points examined on the plane, is less than 30%, whereas for the three-body problem this proportion is almost 100%. The algorithm converges faster in the RTBP problem than in the 2+2 BP. This means that the method needs more iterations (steps) in the latter problem to converge, increasing in this way the computational cost.

(II) Comments Concerning the Equilibrium States of the Two Minor Bodies. Two pairs of the existing 14 equilibrium solutions are evolved in the neighborhood of each collinear Lagrangian point and on both sides of it (collinear positions).

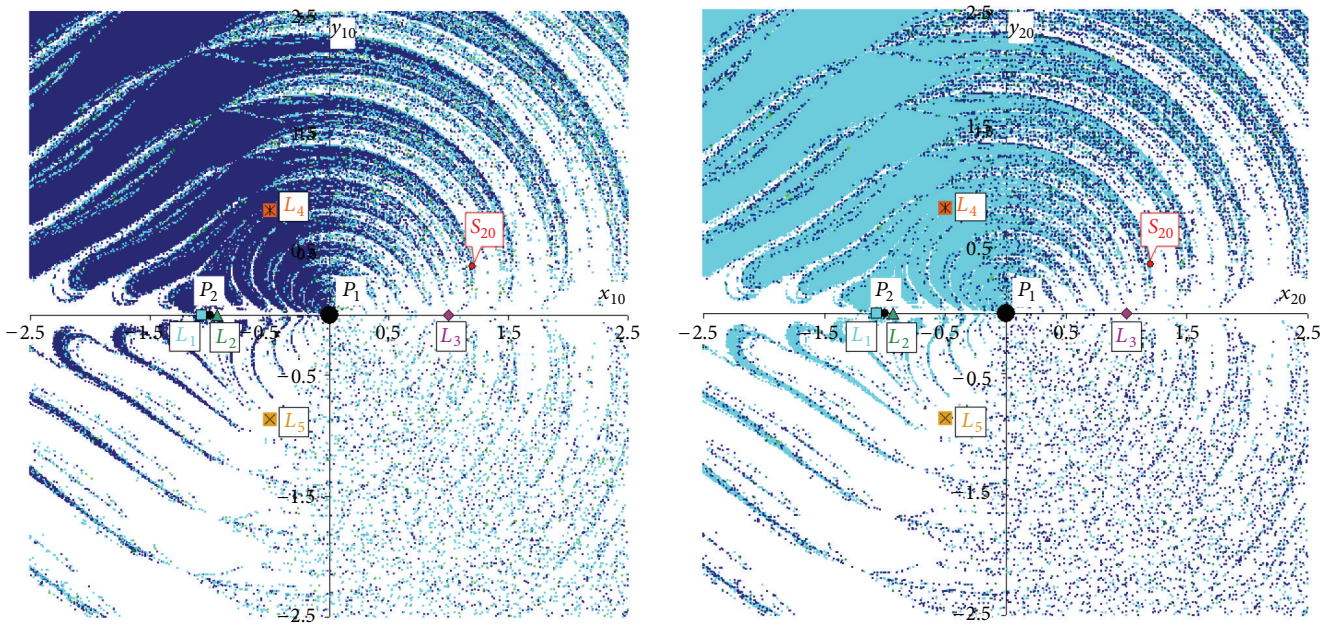

(a) (b)

FIGURE 12: Attracting subsets of the inline and the perpendicular equilibria around L_4 (a) when S_{20} is constant and (b) when S_{10} is constant for the Sun-Jupiter-binary asteroids system.

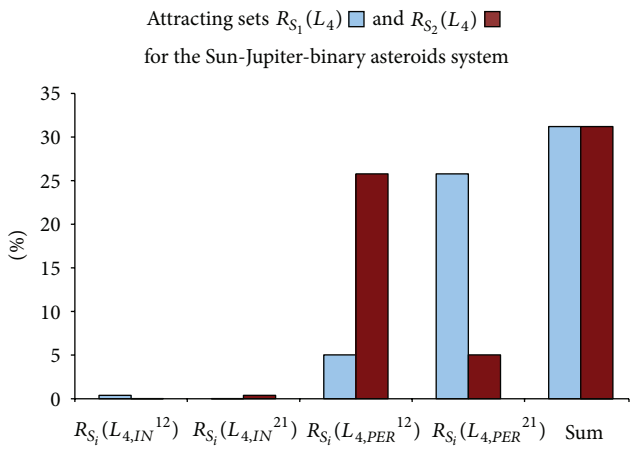

FIGURE 13: Number of points of the attracting subsets $R_{S_i}(L_4)$, $i = 1, 2$, of the inline and the perpendicular equilibria around L_4 as a fraction of the total number of initial values, for the Sun-Jupiter-binary asteroids system.

The remaining four pairs evolve near a triangular Lagrangian point (inline and perpendicular equilibria). The inline points are located on a straight line which passes through point L_4 (or L_5) and forms a small angle φ with the line which connects the triangular Lagrangian point with the origin O. The collinear solutions are unstable for every value of the mass parameters. The same occurs to the inline triangular solutions, where for every set of values of the three mass parameters all the inline triangular equilibrium points are unstable. On the contrary, the perpendicular solutions can be stable for small values of the mass parameter μ.

The distances of all the equilibrium positions from their neighboring Lagrangian points, except for those of the perpendicular ones, slightly change when μ varies in the range $0 < \mu \leq 0.5$. On the contrary, the distances of the perpendicular points from their neighboring triangular Lagrangian ones decrease exponentially with μ. When the masses of the minor bodies vary, their distances from the Lagrangian points change as well. We additionally observe an accumulation of these curves as the two masses μ_1, μ_2 decrease.

As μ increases, the declination angle φ of the inline points also varies. This variation can be expressed by means of a polynomial of 4th degree.

(III) Comments Concerning the Evolution of the Attracting Regions. The attracting regions of the equilibrium states offer an additional aspect of the qualitative characteristics of the nonlinear dynamical system, since they are formed with the use of the expressions of the potential function and its first and second partial derivatives. Whatever the numerical method is, the structure of the attracting regions shows all the symmetry characteristics of the dynamical system. Furthermore, they provide us with the necessary information concerning the suitable initial values which reduce the whole computational cost and minimize the errors during calculations.

For comparison reasons we have investigated the attracting regions of both the restricted three-body problem and the restricted 2+2 BP. Comparing the results obtained by the

two problems we confirm similarities and differences. Among these similarities, we refer to the ones concerning that in both problems the attracting region $R(L_4)$ of the RTBP and the attracting set $R_{S_i}(L_4)$ of the 2+2 BP are the biggest and the more extended ones, while the attracting region $R(L_1)$ of the RTBP and the attracting set $R_{S_i}(L_4)$ of the 2+2 BP occupy the smallest area of all the basins for every value of the parameters μ $(0 < \mu \leq 0.5)$, μ_1, μ_2. The most remarkable difference is that the "compact" areas of an attracting region in the RTBP are more extended than the corresponding ones in the 2+2 BP, where they appear as tiny islands in the searching area, thus making the finding of the equilibrium locations in the latter problem more difficult.

Appendix

A. Sun-Jupiter-Binary Asteroids System

Mass of the Sun: $M_S = 1.99 \cdot 10^{30}$ Kg.

Mass of Jupiter: $M_J = 1.9 \cdot 10^{27}$ Kg.

Mean distance of Jupiter from Sun: 5.2 AU = 777920000 km.

Reduced mass of Jupiter: $\mu = M_J/(M_S + M_J) = 0.0009538754$.

Mass of S_1: $m_1 = 1.59352 \cdot 10^{15}$ Kg.

Reduced mass of S_1: $\mu_1 = 8 \cdot 10^{-16}$.

Mass of S_2: $m_2 = 3.9838 \cdot 10^{14}$ Kg.

Reduced mass of S_2: $\mu_2 = 2 \cdot 10^{-16}$.

Reduced mass of S_2, $\mu' = \mu_2/(\mu_1 + \mu_2)$: $\mu' = 0.2$.

B. Earth-Moon-Dual Satellite System

Mass of the Earth: $M_\oplus = 5.98 \cdot 10^{24}$ Kg.

Mass of the Moon: $M_C = 7.35 \cdot 10^{22}$ Kg.

Mean distance of the Moon from Earth: 384400 km.

Reduced mass of the Moon: $\mu = M_C/(M_\oplus + M_C) = 0.012141736185$.

Mass of S_1: $m_1 = 475$ Kg.

Reduced mass of S_1: $\mu_1 = m_1/(M_\oplus + M_C) = 7.8467 \cdot 10^{-23}$.

Mass of S_2: $m_2 = 245$ Kg.

Reduced mass of S_2: $\mu_2 = m_2/(M_\oplus + M_C) = 4.0472 \cdot 10^{-23}$.

Reduced mass of S_2: $\mu' = \mu_2/(\mu_1 + \mu_2)$: $\mu' = 0.34027$.

References

[1] A. L. Whipple, "Equilibrium solutions of the restricted problem of 2+2 bodies," *Celestial Mechanics*, vol. 33, pp. 271–294, 1984.

[2] A. L. Whipple and L. K. White, "Stability of binary asteroids," *Celestial Mechanics*, vol. 35, no. 1, pp. 95–104, 1985.

[3] A. Milani and A. Nobili, "Instability of the 2+2 body problem," *Celestial Mechanics*, vol. 41, pp. 153–160, 1988.

[4] D. Thanos, "Regularization of the gravitational restricted planar 2+2 problem for collisions between minors," *The Astronomical Journal*, vol. 97, pp. 1220–1226, 1989.

[5] S. M. El-Shaboury, "Equilibrium solutions of the restricted problem of 2+2 axi-symmetric rigid bodies," *Celestial Mechanics*, vol. 50, pp. 199–208, 1991.

[6] D. G. Michalakis and A. G. Mavraganis, "The equilibrium configurations of the restricted problem of 2+2 triaxial rigid bodies," *Celestial Mechanics & Dynamical Astronomy*, vol. 63, no. 1, pp. 81–100, 1995.

[7] T. J. Kalvouridis and A. G. Mavraganis, "Equilibria and stability of the restricted photogravitational problem of 2+2 bodies," *Astrophysics and Space Science*, vol. 226, no. 1, pp. 137–148, 1995.

[8] A. G. Mavraganis and T. J. Kalvouridis, "Equilibrium attitudes of two gyrostats in syzygy with two attracting centers," in *Proceedings of the 2nd Astronomical Conference*, pp. 609–614, Thessaloniki, Greece, 1996.

[9] T. J. Kalvouridis, "The oblate spheroids version of the restricted photogravitational 2+2 body problem," *Astrophysics and Space Science*, vol. 246, no. 2, pp. 219–227, 1997.

[10] A. Prasad and B. Ishwar, "Equations of motion of the restricted problem of (2+2) bodies when primaries are magnetic dipoles and minor bodies are taken as electric dipoles," *Celestial Mechanics and Dynamical Astronomy*, vol. 64, no. 4, pp. 305–312, 1996.

[11] A. L. Whipple and V. Szebehely, "The restricted problem of n+ν bodies," *Celestial Mechanics*, vol. 32, no. 2, pp. 137–144, 1984.

[12] V. Szebehely, *Theory of Orbits*, Academic Press, New York, NY, USA, 1967.

[13] M. N. Croustalloudi and T. J. Kalvouridis, "On the structure and evolution of the "Basins of Attraction" in ring-type N-body formation," in *Order and Chaos in Stellar and Planetary Systems*, G. Byrd, K. Kholshevnikov, A. Myllari, I. Nikiforov, and V. Orlov, Eds., vol. 316 of *ASP Conference Series*, pp. 93–96, 2004.

[14] M. N. Croustalloudi and T. J. Kalvouridis, "Attracting domains in ring-type N-body formations," *Planetary and Space Science*, vol. 55, no. 1-2, pp. 53–69, 2007.

[15] H. Peitgen, H. Jurgens, and D. Saupe, *Chaos and Fractals*, Springer, New York, NY, USA, 1992.